Coleman et al., 2018, How, where, and when do radial faults grow near salt diapirs?: Geology, https://doi.org/10.1130/G40338.1.

APPENDIX DR1. AVERAGE VERTICAL SEISMIC RESOLUTION

Average vertical seismic resolution (red solid line) with depth using a velocity of ~ 2 km/s (after Jackson et al., 2014) and the frequency (black dashed line). The average vertical seismic resolution was calculated using the frequency and velocity. The instantaneous frequency is shown (left). Vertical exaggeration ~ 4.5.

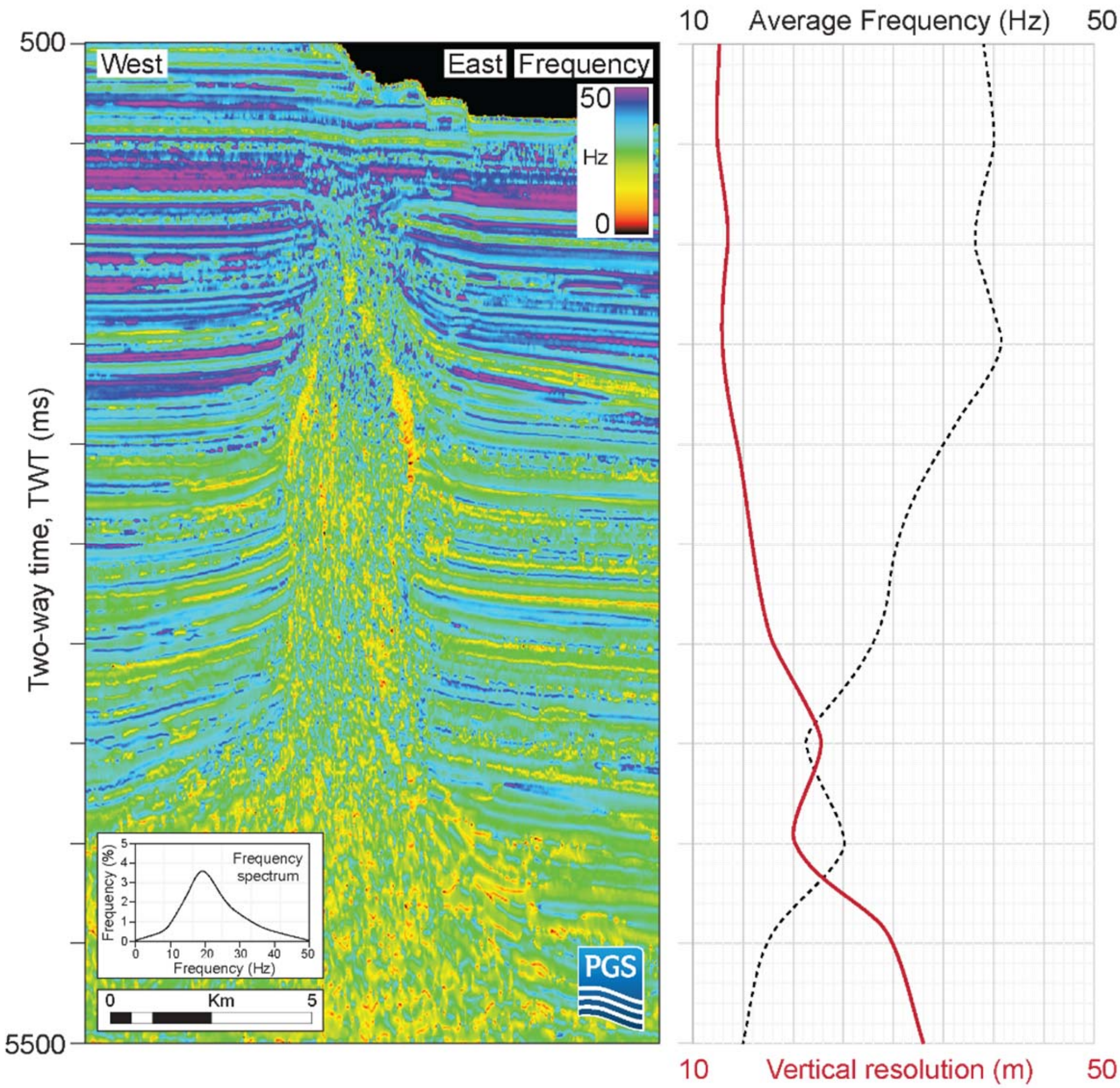

APPENDIX DR2. QUANTITATIVE THROW ANALYSIS METHOD

Fault throw was measured perpendicular to radial fault strike every c. 50 – 100 m along the length of individual radial faults using horizon cut-offs (e.g. Muraoka and Kamata, 1983; Baudon and Cartwright, 2008). Cut-offs were defined using an extrapolated line that follows the regional trend of the chosen horizon prior to folding (Wilson et al., 2013), removing the effect of fault-parallel folding (Walsh et al., 1996). Therefore, total strain across the fault is accommodated, whether accommodated by ductile (continuous) or brittle (discontinuous) deformation (e.g. Long and Imber, 2010). The throw maxima was then identified on each radial fault, and plotted as white squares on Fig. 3. Fault throw was also measured with depth (T-z plots) using the aforementioned cut-offs, and throw maxima marked by white squares on Fig. 4.

Expansion indices illustrate variations in sediment thickness adjacent to fault systems, revealing the kinematics of bounding faults (e.g. Thorsen, 1963; Tvedt et al., 2013; Jackson et al., 2017). Expansion indices were calculated by dividing the hangingwall thickness of a stratal units by its corresponding footwall thickness and plotting these against geological time. An expansion index of 1 suggests no across-fault thickening, and a lack of syndepositional fault activity. An index of >1 suggests across-fault thickening and syndepositional fault activity. An index of <1 suggests stratal thinning from the footwall to the hangingwall, and may reflect difficulties in accurately measuring stratal thicknesses adjacent to a fault. Expansion indices near vertical fault tips may be slightly above and below one (± 0.1) due to ductile deformation (e.g. Barnett et al., 1987). T1 – T4 represent horizon tops. The white circle represents the vertical fault tip.

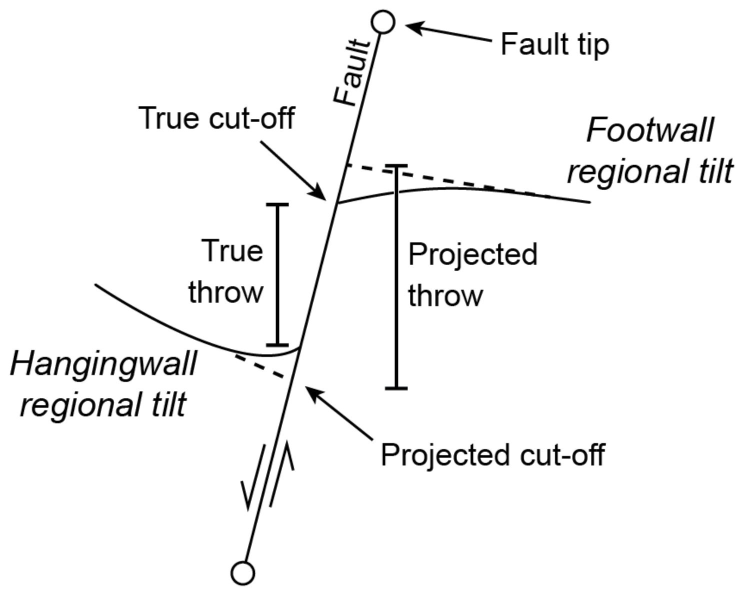
Fault tip
Fault
True cut-off
Footwall
regional tilt
True
throw
Projected
throw
Hangingwall
regional tilt
Projected cut-off

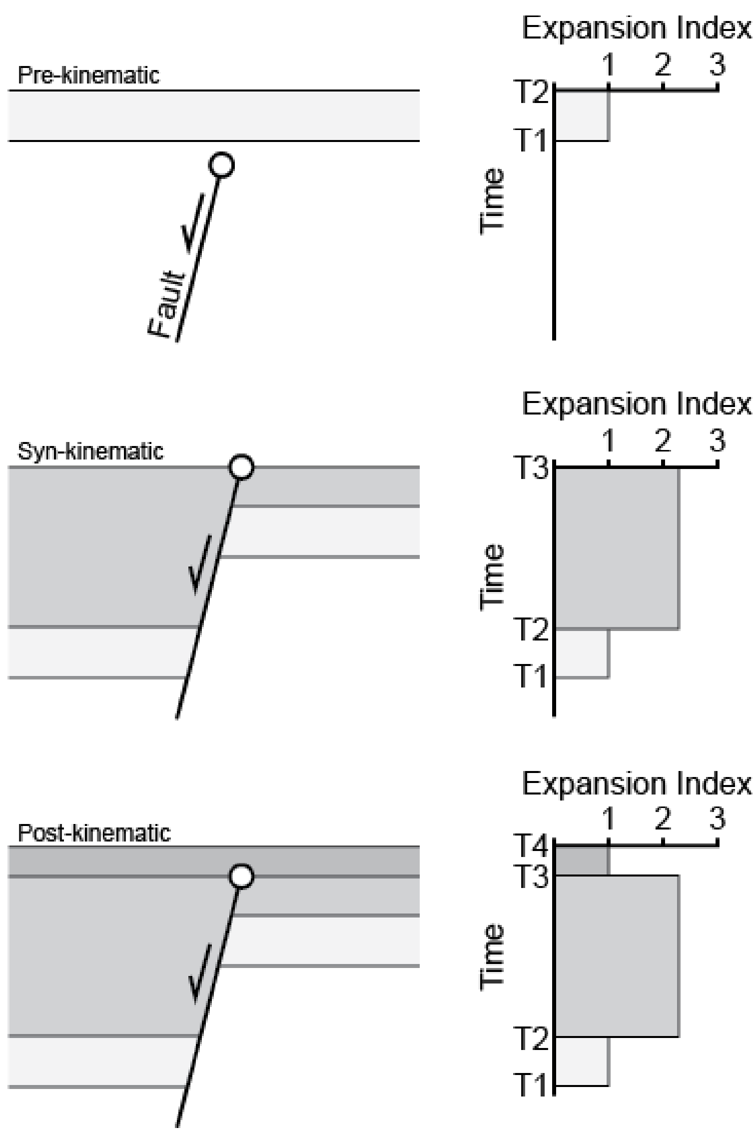
Pre-kinematic
Fault
Expansion Index
1 2 3
T2
T1
Time
Syn-kinematic
Expansion Index
1 2 3
T3
T2
T1
Time
Post-kinematic
Expansion Index
1 2 3
T4
T3
T2
T1
Time

References for Appendix DR2


Barnett, J. A., Mortimer, J., Rippon, J. H., Walsh, J. J., and Watterson, J., 1987, Displacement geometry in the volume containing a single normal fault: AAPG Bulletin, v. 71, no. 8, p. 925-937.

Baudon, C., and Cartwright, J. A., 2008, 3D seismic characterisation of an array of blind normal faults in the Levant Basin, Eastern Mediterranean: Journal of Structural Geology, v. 30, no. 6, p. 746-760.

Jackson, C. A.-L., Bell, R. E., Rotevatn, A., and Tvedt, A. B. M., 2017, Techniques to determine the kinematics of synsedimentary normal faults and implications for fault growth models: Geological Society, London, Special Publications, v. 439.

Long, J., and Imber, J., 2010, Geometrically coherent continuous deformation in the volume surrounding a seismically imaged normal fault-array: Journal of Structural Geology, v. 32, no. 2, p. 222-234.

Muraoka, H., and Kamata, H., 1983, Displacement distribution along minor fault traces: Journal of Structural Geology, v. 5, no. 5, p. 483-495.

Thorsen, C. E., 1963, Age of growth faulting in southeast Louisiana.

Tvedt, A. B. M., Rotevatn, A., Jackson, C. A. L., Fossen, H., and Gawthorpe, R. L., 2013, Growth of normal faults in multilayer sequences: A 3D seismic case study from the Egersund Basin, Norwegian North Sea: Journal of Structural Geology, v. 55, p. 1-20.

Walsh, J. J., Watterson, J., Childs, C., and Nicol, A., 1996, Ductile strain effects in the analysis of seismic interpretations of normal fault systems: Geological Society, London, Special Publications, v. 99, no. 1, p. 27-40.

Wilson, P., Elliott, G. M., Gawthorpe, R. L., Jackson, C. A.-L., Michelsen, L., and Sharp, I. R., 2013, Geometry and segmentation of an evaporite-detached normal fault array: 3D seismic analysis of the southern Bremstein Fault Complex, offshore mid-Norway: Journal of Structural Geology, v. 51, p. 74-91.

APPENDIX DR3. FAULT THROW RESOLUTION

Fault throw resolution for an example radial fault at Santos. Although vertical resolution may decrease with depth, the vertical offset between amplitude peaks between adjacent seismic traces permits fault throw to be measured to c. 5ms at shallow depths (< 3000 ms TWT). However, at greater depths (>3000 ms TWT), the peaks of individual traces become increasingly smeared as the vertical resolution decreases, and as such, vertical offsets are less distinct and measurement becomes increasingly difficult.

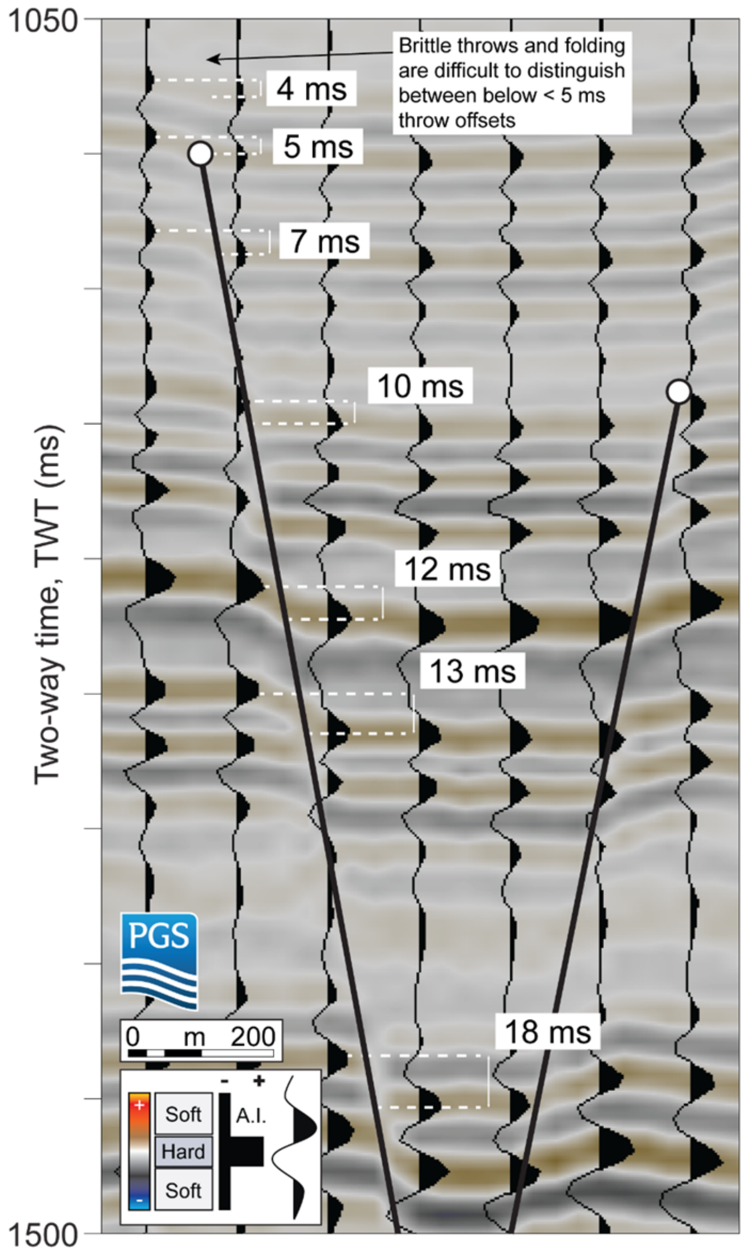

APPENDIX DR4. ASPECT RATIO FOR SANTOS BASIN RADIAL FAULTS

Aspect ratios for Santos Basin radial faults. Velocity ~ 2km/s after Jackson et al. (2014).

| Fault # | Max Length (m) | Height (m) | Aspect Ratio |
|---|---|---|---|
| 1 | 3727 | 871 | 4.28 |
| 2 | 704 | 596 | 1.18 |
| 3 | 639 | 639 | 0.69 |
| 4 | 2021 | 811 | 2.49 |
| 5 | 1340 | 809 | 1.66 |
| 6 | 1131 | 655 | 1.73 |
| 7 | 601 | 361 | 1.66 |
| 8 | 2909 | 1521 | 1.91 |
| 9 | 1075 | 434 | 2.48 |
| 10 | 1732 | 650 | 2.66 |
| 11 | 644 | 557 | 1.16 |
| 12 | 1536 | 923 | 1.66 |
| 13 | 833 | 833 | 0.72 |
| 14 | 1542 | 620 | 2.49 |
| 15 | 1826 | 683 | 2.67 |
| 16 | 1100 | 208 | 5.29 |
| 17 | 1742 | 666 | 2.62 |
| 18 | 1322 | 500 | 2.64 |
| 19 | 2001 | 736 | 2.72 |
| 20 | 809 | 545 | 1.48 |
| 21 | 579 | 579 | 0.78 |
| 22 | 1246 | 275 | 4.53 |
| 23 | 1969 | 501 | 3.93 |
| 24 | 947 | 323 | 2.93 |
| 25 | 2585 | 676 | 3.82 |
| 26 | 882 | 735 | 1.20 |
| 27 | 1726 | 669 | 2.58 |
| 28 | 1490 | 731 | 2.04 |
| 29 | 1713 | 368 | 4.65 |
| 30 | 600 | 580 | 1.03 |
| 31 | 1146 | 663 | 1.73 |
| 32 | 644 | 579 | 1.11 |
| 33 | 1471 | 782 | 1.88 |
| 34 | 1004 | 350 | 2.87 |
| 35 | 412 | 412 | 0.90 |
| 36 | 754 | 496 | 1.52 |
| 37 | 903 | 670 | 1.35 |
| 38 | 2510 | 401 | 6.26 |
| 39 | 1457 | 693 | 2.10 |
| 40 | 464 | 464 | 0.82 |
| 41 | 726 | 726 | 0.52 |

| | | | |
|---|---|---|---|
| 42 | 540 | 540 | 0.92 |
| 43 | 955 | 685 | 1.39 |
| 44 | 856 | 657 | 1.30 |
| 45 | 1328 | 493 | 2.69 |
| 46 | 1072 | 734 | 1.46 |
| 47 | 791 | 726 | 1.09 |
| 48 | 1619 | 566 | 2.86 |
| 49 | 1580 | 551 | 2.87 |
| 50 | 1276 | 707 | 1.80 |
| 51 | 1288 | 463 | 2.78 |
| 52 | 859 | 701 | 1.23 |
| 53 | 1764 | 699 | 2.52 |
| 54 | 1090 | 480 | 2.27 |
| 55 | 964 | 596 | 1.62 |
| 56 | 754 | 754 | 0.88 |

APPENDIX DR5. CIRCUMFERENTIAL SEISMIC SECTIONS

Circumferential seismic sections parallel to the salt-sediment interface documenting the different vertical tiers of radial faults around the isolated salt stock. H1 – 3 and Faults 1 - 4 are also shown.

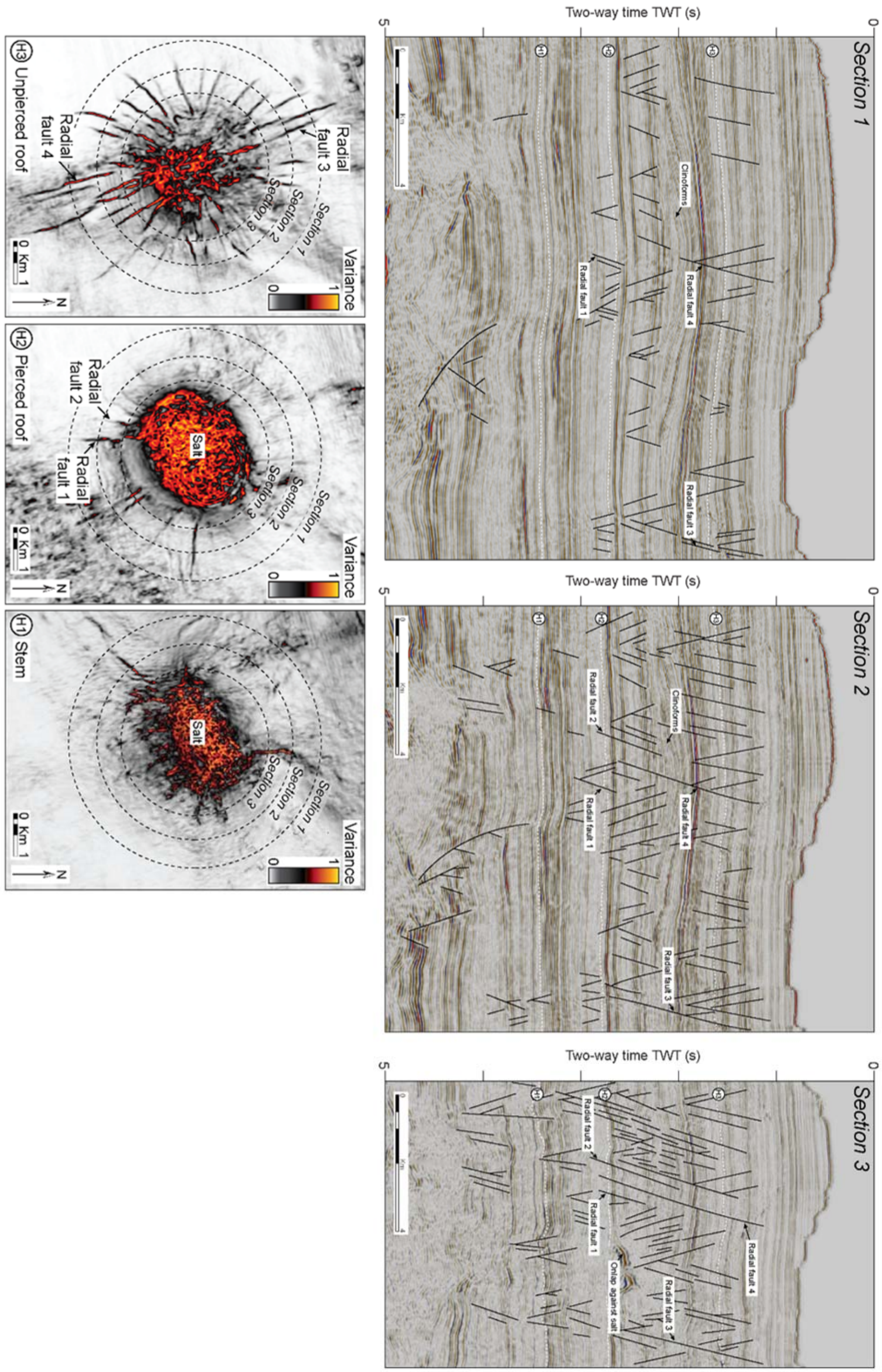

APPENDIX DR6. RADIAL FAULT THROW FOR H2-3

Throw-distance on Fig. 3 used to determine the position of throw maxima along-strike for H2 - 3. Radial fault throw (i.e. strain) generally increases towards the diapir in H1 and H2.

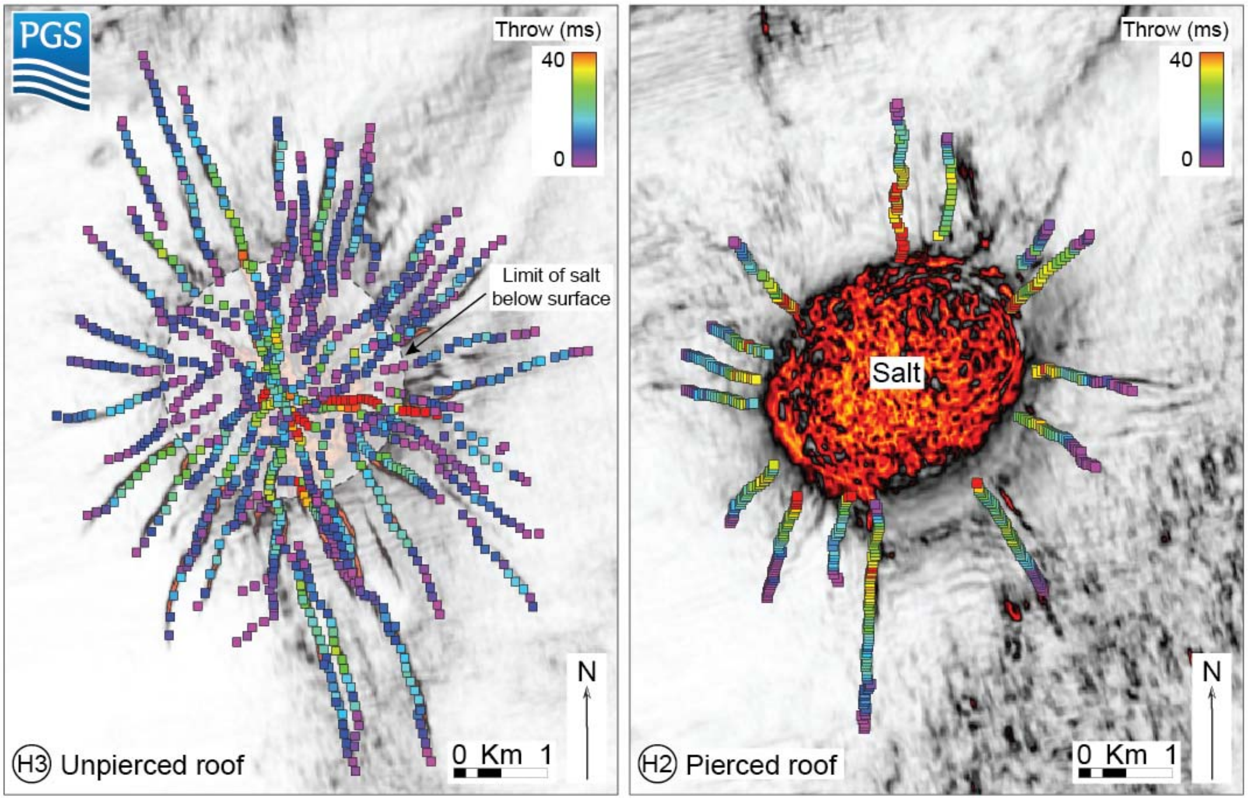

APPENDIX DR7. UPPER THROW TIP GRADIENTS

Upper throw tip gradients for the Santos Basin radial faults.

| Fault | Throw (m) | Upper tip radius (m) | Vertical tip throw gradient |
|---|---|---|---|
| 1 | 47 | 494 | 0.09 |
| 2 | 32 | 308 | 0.10 |
| 3 | 25 | 350 | 0.07 |
| 4 | 25 | 281 | 0.09 |
| 5 | 25 | 202 | 0.12 |
| 6 | 20 | 139 | 0.14 |
| 7 | 26 | 197 | 0.13 |
| 8 | 23 | 499 | 0.05 |
| 9 | 23 | 233 | 0.10 |
| 10 | 21 | 303 | 0.07 |
| 11 | 36 | 322 | 0.11 |
| 12 | 37 | 507 | 0.07 |
| 13 | 21 | 123 | 0.17 |
| 14 | 16 | 151 | 0.11 |
| 15 | 15 | 66 | 0.23 |
| 16 | 29 | 254 | 0.11 |
| 17 | 38 | 368 | 0.10 |
| 18 | 30 | 307 | 0.10 |
| 19 | 24 | 126 | 0.19 |
| 20 | 20 | 338 | 0.06 |
| 21 | 20 | 147 | 0.14 |
| 22 | 20 | 305 | 0.07 |
| 23 | 20 | 469 | 0.04 |
| 24 | 20 | 454 | 0.04 |

| | | | |
|---|---|---|---|
| 25 | 66 | 515 | 0.13 |
| 26 | 60 | 499 | 0.12 |
| 27 | 22 | 125 | 0.18 |
| 28 | 22 | 206 | 0.11 |
| 29 | 23 | 310 | 0.07 |
| 30 | 22 | 427 | 0.05 |
| 31 | 21 | 312 | 0.07 |
| 32 | 19 | 231 | 0.08 |
| 33 | 19 | 194 | 0.10 |
| 34 | 22 | 396 | 0.06 |
| 35 | 24 | 250 | 0.09 |
| 36 | 21 | 335 | 0.06 |
| 37 | 14 | 284 | 0.05 |
| 38 | 18 | 247 | 0.07 |
| 39 | 21 | 248 | 0.08 |
| 40 | 18 | 337 | 0.05 |